The Influence of Chromium on Mechanical Properties of Austempered Ductile Cast Iron

L. Bartosiewicz, I. Singh, F.A. Alberts, A.R. Krause, and S.K. Putatunda

An investigation was carried out to examine the influence of microstructure and chromium on the tensile properties and plane strain fracture toughness of austempered ductile cast iron (ADI). The investigation also examined the growth kinetics of ferrite in these alloys. Compact tension and round cylindrical tensile specimens were prepared from ductile cast iron with Cr as well as without Cr. These specimens were then given four different heat treatments to produce four different microstructures. Tensile tests and fracture toughness tests were carried out as per ASTM standards E-8 and E-399. The crack growth mechanism during fracture toughness tests was also determined.

The test results indicate that yield strength, tensile strength, and fracture toughness of ADI increases with an increase in the volume fractions of ferrite, and the fracture toughness reaches a peak when the volume fractions of the ferrite are approximately 60% in these alloys. The Cr addition was found to reduce the fracture toughness of ADI at lower hardness levels (<40 HRC); at higher hardness levels (≥40 HRC), the effect of chromium on the fracture toughness was negligible. The crack growth mechanism was found to be a combination of quasi-cleavage and microvoid coalescences, and the crack trajectories connect the graphite nodules along the way.

Keywords

mechanical properties, austempered ductile cast iron, fracture toughness, phase transformation

1. Introduction

IN RECENT years, there has been significant interest in processing and developing austempered ductile cast iron (ADI). Many workers have reported excellent mechanical properties (Ref 1-5) of properly cast and heat treated ADI. It appears that ADI can be developed into a major engineering material with a wide range of versatile properties.

ADI is a heat treated alloyed nodular cast iron with a unique microstructure that consists of high carbon austenite (γ_{HC}) and acicular ferrite (α) with graphite nodules dispersed in it. This structure, in ADI produces very good mechanical properties. It had high strength and low weight and, ADI has good wear resistance (Ref 6), excellent damping capacity (Ref 7), and good thermal conductivity (Ref 8), and these properties are superior to those of plain carbon and low alloy steels. ADI is also highly versatile with respect to manufacturing; the cost of an ADI component is lower (Ref 9) than low alloy and plain carbon steels.

ADI has a composition which is very similar to that of nodular or ductile cast iron. Usually, some alloying elements, such as nickel, molybdenum, and copper, are added to widen the process window, i.e., to delay the austenite decomposition (Ref 10, 11) into pearlite and ferrite upon cooling. Proper casting and austempering heat treatment will prevent the formation of detrimental microstructural constituents, such as pearlite, bainite, martensite, or carbide. Incidentally, improper casting practices can produce these unwanted microstructural constituents, and these cannot be eliminated with the normal heat treatment practice.

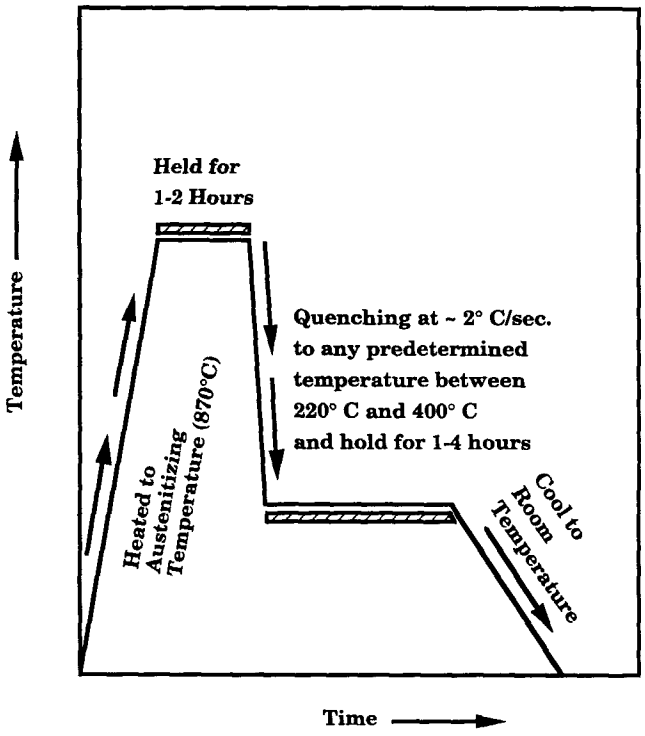

Fig. 1 Schematic diagram of ADI heat treatment process.

L. Bartosiewicz, Staff Scientist, Scientific Research Laboratories, Ford Motor Company, Dearborn, MI 48121, USA; **I. Singh,** Graduate Research Assistant, Department of Materials Science and Engineering, Wayne State University, Detroit, MI 48202, USA; **F.A. Alberts,** Research Engineer, Scientific Research Laboratories, Ford Motor Company, Dearborn, MI 48121, USA; **A.R. Krause,** Research Scientist, Senior, Scientific Research Laboratories, Ford Motor Company, Dearborn, MI 48121, USA; and **S.K. Putatunda,** Associate Professor, Department of Materials Science and Engineering, Wayne State University, Detroit, MI 48202, USA.

Table 1 Chemical composition of ADI-1 and ADI-2

Element	Composition, wt %
ADI-1 (heat treated conditions A, B, C, D)	
C	3.5
Mn	0.4
Si	2.65
Mg	0.035
S	0.01
P	0.021
Ni	1.6
Ti	0.02
Mo	0.3
Cr	nil
Cu	0.055
V	0.05
ADI-2 (heat treated conditions G, H, I, J)	
C	3.5
Mn	0.38
Si	2.47
Mg	0.035
S	0.01
P	0.021
Ni	1.57
Ti	0.02
Mo	0.30
Cr	0.50
Cu	0.35
V	0.05

Table 2 Heat treatment procedure for ADI-1 and ADI-2

Heat treated condition	Austempering temperature, °C	Austempering time, h
ADI-1		
A	273	3.5
B	329	2.5
C	366	2.0
D	385	2.0
ADI-2		
G	260	4
H	288	3.5
I	358	2.5
J	385	2

For the development of ADI, a two-step process is required. The first step is the melting and casting of alloyed nodular ductile cast iron. This step is followed by heat treatments. Figure 1 shows a schematic of the heat treatment cycle. The casting is heated and held at the temperature range of 840 to 900 °C for 1 to 2 h depending upon the chemical composition and section size. (Alloys with conventional composition will have to be heat treated for a longer period if the section thickness exceeds 2 in. Similarly, austempering time and temperature will be different for alloys with different chemical compositions.) At this stage, the structure becomes fully austenitized (γ). After austenitizing, the alloy is immediately quenched in a molten salt bath and held at the austempering temperature range of 220 to 400 °C. The casting is maintained at this temperature range for 2 to 4 h and then air cooled to room temperature.

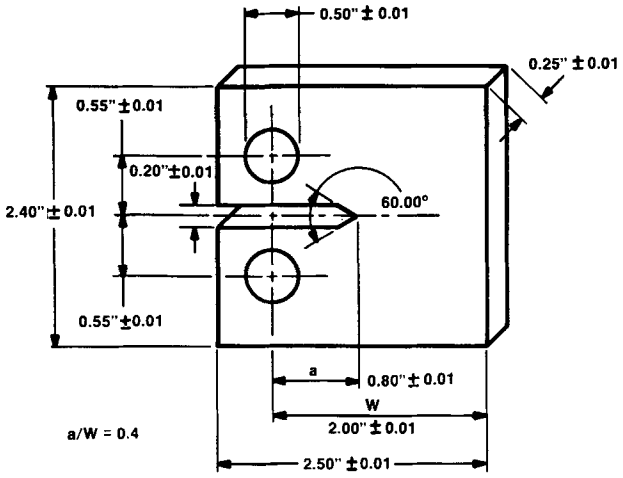

Compact Tension Specimen

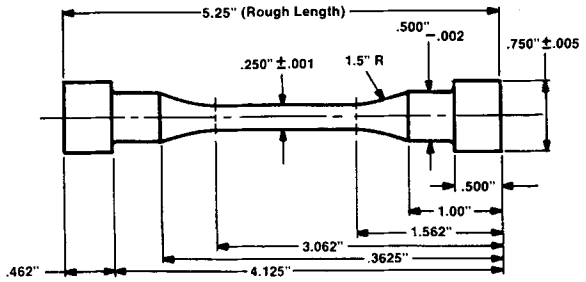

Tensile Specimen

Fig. 2 Schematics of test specimens.

During the austempering process, ADI undergoes a two-stage transformation process (Ref 12, 13). In the first stage, the austenite (γ) decomposes into ferrite (α) and high carbon or carbon saturated austenite (γ_{HC}). This reaction can be expressed as:

$$\gamma \rightarrow \alpha + \gamma_{HC} \quad \text{(Eq 1)}$$

If the casting is held at the austempering temperature for too long (Ref 11), then the carbon supersaturated austenite (γ_{HC}) further decomposes into ferrite (α) and carbide (ε), i.e.,

$$\gamma_{HC} \rightarrow \alpha + \varepsilon \quad \text{(Eq 2)}$$

In this case, the alloy will contain large amounts of ε carbide, which makes the material very brittle (Ref 13). This reaction is, therefore, undesirable and must be avoided. The optimum mechanical properties (strength, ductility, toughness) are achieved upon completion of the first reaction but before the onset of the carbide forming reaction. The microstructure of ADI can be widely altered by suitable heat treatments, i.e., de-

Table 3 Mechanical properties of ADI-1 and ADI-2

Material condition	Yield strength, MPa	Ultimate tensile strength, MPa	Elongation, %	Reduction in area, %	Hardness, HRC
As-cast ADI-1	504	630	5.5	6.90	24 ± 1
As-cast ADI-2	510	625	5.5	7.0	23 ± 1
Heat treated condition A	1137	1179	0.80	1.20	45 ± 2
Heat treated condition G	1250	1438	1.6	0.9	48 ± 2
Heat treated condition B	1103	1144	1.05	1.04	40 ± 2
Heat treated condition H	990	1130	2.3	11.6	45 ± 2
Heat treated condition C	970	1010	1.40	1.60	35 ± 2
Heat treated condition I	750	980	3.8	2.3	35 ± 2
Heat treated condition D	595	848	5.1	4.10	30 ± 2
Heat treated condition J	650	830	5.1	5.5	32 ± 2

pending upon austempering time and temperature, different volume fractions of austenite and ferrite will be produced in the alloy. These microstructural components regulate the mechanical properties of the alloy.

The microstructure of an alloy has a strong influence on mechanical properties and fracture toughness. Plane strain fracture toughness, K_{Ic} (Ref 14), is a measure of the resistance of the material to crack growth under a sustained monotonic loading condition. Fracture toughness is an extremely important parameter for structural design since structural components designed on the basis of fracture toughness are expected to survive in service without catastrophic failure. Fracture toughness depends on the microstructure (Ref 15, 16) of the material, and microstructural modification appears to be the only possible way to improve the fracture toughness. Since the microstructure in ADI consists mainly of ferrite and carbon saturated austenite, it could be possible to improve the fracture toughness of ADI with a heat treatment process, i.e., by changing the volume fractions of the major phases. Furthermore, alloying elements can influence the fracture and tensile properties of an alloy. However, very little is known about the specific influence of Cr on the fracture toughness or on the tensile properties of austempered ductile cast iron.

The present investigation was undertaken to determine the influence of microstructure and chromium on the tensile properties and plane strain fracture toughness (K_{Ic}) of ADI. Conventional ductile cast iron (ADI-1) (with Ni and Mo) and ADI alloyed with chromium (ADI-2) were used in this study. These ADI alloys were heat treated with four different conditions to produce four different microstructures. The growth kinetics of ferrite in these alloys were also examined and ascertained by image analysis and scanning electron microscopy (SEM) studies. Tensile properties and the plane strain fracture toughness of these materials were evaluated as a function of austempering temperature and microstructure. The crack growth mechanism during fracture toughness tests was also determined through fractographic analysis of the fracture surfaces.

2. Experimental Procedure

2.1 *Material*

ADI of two different chemical compositions (ADI-1 and ADI-2) was used in this study; the castings were made using preheated ladles and molds to avoid detrimental microstructures. The first material (ADI-1) used in this investigation is a conventional ductile cast iron containing usual alloying elements, i.e., nickel and molybdenum. The second material (ADI-2) contained an additional 0.5 wt% chromium. The chemical compositions of these alloys are reported in Table 1. These materials were cast in 370-mm by 100-mm by 75-mm (14-in. × 4-in. × 3-in.) flat bar stocks. From these stocks, two types of specimens were prepared, i.e., round cylindrical specimens for tensile tests and compact tension specimens for fracture toughness tests. The tensile specimens were prepared as per ASTM standard E-8 (Ref 17), whereas the compact tension specimens were prepared as per ASTM standard E-399 (Ref 14). The width (W) of these specimens was 50.8 mm (2 in.), and the thickness (B) was 25.4 mm (1 in.). The aspect ratio was kept at a/W = 0.45. The specimens had specially prepared knife edge slots for insertion of the clip gages to monitor the load and displacement during fracture toughness tests. After fabrication, the specimens were x-rayed, and only defect-free samples were selected for subsequent heat treatments, tensile testing, and fracture toughness testing. Schematics of both compact tension and tensile specimens are shown in Fig. 2.

After the fabrication, the compact tension as well as the tensile specimens were heat treated with four different heat treatments. These heat treated conditions (Table 2) are identified as A, B, C, and D for ADI-1 and G, H, I, and J for ADI-2. All these specimens were initially austenitized at 871 °C for two hours and then immediately austempered in a molten salt bath for different time periods at different temperatures. The details of these heat treatments are reported in Table 2. The tensile properties of ADI-1 and ADI-2 in as-cast as well as after four different heat treated conditions were determined according to ASTM standard E-8 (Ref 17). Three to four identical test specimens were used from each group of ADI-1 and ADI-2 and from each heat treated condition. The average values are reported in Table 3. The microstructure of the materials in the different heat treated conditions, A, B, C, and D, are shown in Fig. 3(a), (b), (c), and (d). Conditions G, H, I, and J are shown in Fig. 4(a), (b), (c), and (d), respectively. In these figures, the austenite appears as light gray, and the ferrite as dark. The volume fractions of these phases as well as the spacing between the graphite nodules were determined using an image analyzer. The average values for the volume fractions of phases for the heat treated samples are reported in Table 4.

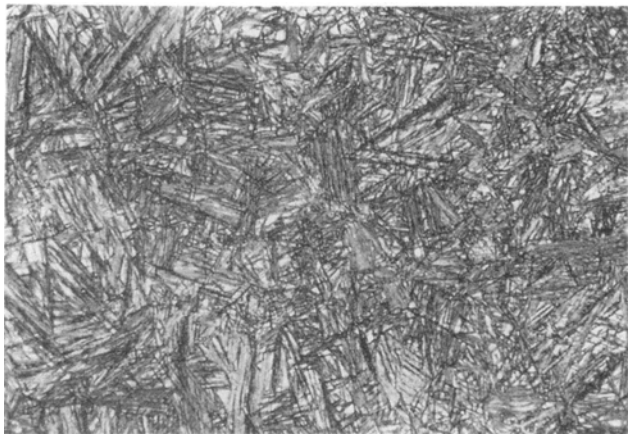

(a)

(b)

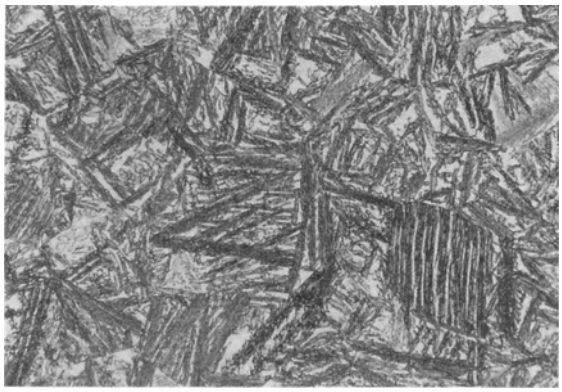

(c)

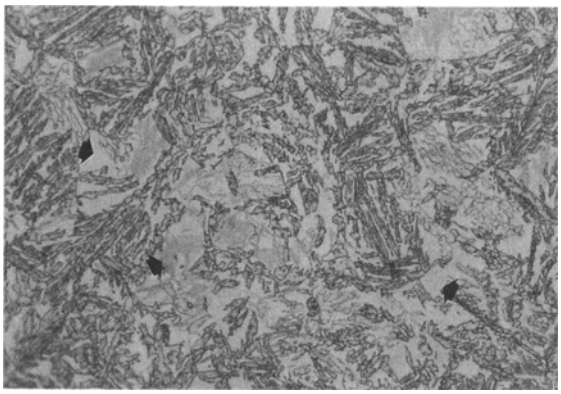

(d)

Fig. 3 Microstructure of ADI without Cr. 1000×. (a) Heat treated condition A. Austempered at 260 °C for 4 h. (b) Heat treated condition B. Austempered at 288 °C for 3.5 h. (c) Heat treated condition C. Austempered at 358 °C for 2.5 h. (d) Heat treated condition D. Austempered at 385 °C for 2 h.

Table 4 Volume fractions of ferrite and austenite in ADI-1 and ADI-2 (tensile and fracture toughness samples)

Material condition	Volume fraction of austenite, %	Volume fraction of ferrite, %	Volume fraction of graphite, %
As-cast ADI-1	Nil (<0.3)	Nil	12
As-cast ADI-2	Nil	Nil	14
Heat treated condition A	12	71	17
Heat treated condition G	13	71	18
Heat treated condition B	25	63	13
Heat treated condition H	26	60	15
Heat treated condition C	36	48	19
Heat treated condition I	35	50	15
Heat treated condition D	53	32	14
Heat treated condition J	44	40	16

2.2 *Fracture Toughness Testing*

After heat treatment, the compact tension specimens were polished to a mirror finish surface using first a 600 grit emery paper and subsequently a 0.3 μm alumina slurry. The specimens were then precracked in fatigue at a ΔK level of 10 MPa$\sqrt{m}$ to produce a 2-mm-long sharp and reproducible crack front as per ASTM standard E-399 (Ref 14). After fatigue precracking, the specimens were loaded in tension, and load-displacement diagrams were obtained with the clip gauge placed in the knife edge attachment of the specimens. From this load-displacement diagram, the P_Q values were calculated using the 5% secant deviation technique. From this P_Q value, the K_Q values were calculated using the standardized calibration function for the stress intensity factor for compact tension specimens (Ref 14). Four to five identical test specimens were tested from each heat treated condition—A, B, C, D, G, H, I, and J. The averages of the experimentally measured values are reported in Table 5. Since the test results satisfied all the conditions of ASTM E-399, the K_Q values obtained were valid K_{Ic} values.

The fractographic samples were prepared for fracture surface analysis and analyzed with a SEM. For the kinetic studies, a separate batch of specimens was prepared from ADI-1 and ADI-2. The specimens were austenitized at a constant tempera-

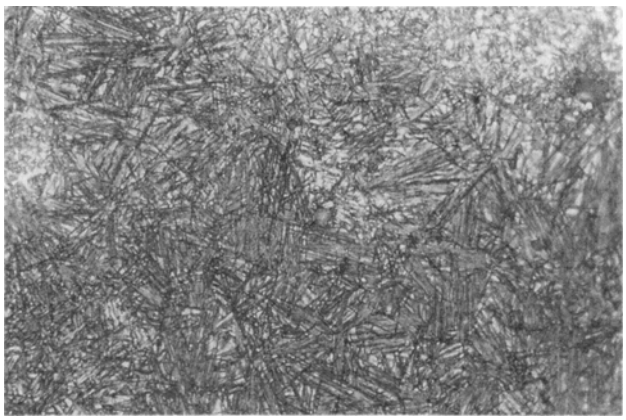

(a)

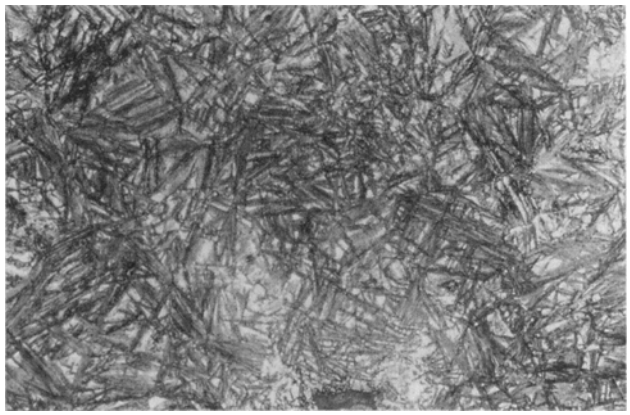

(b)

(c)

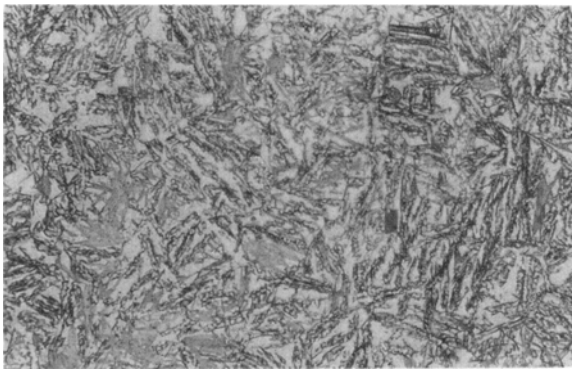

(d)

Fig. 4 Microstructure of ADI with Cr. 1000×. (a) Heat treated condition G. Austempered at 260 °C for 4 h. (b) Heat treated condition H. Austempered at 288 °C for 3.5 h. (c) Heat treated condition I. Austempered at 358 °C for 2.5 h. (d) Heat treated condition J. Austempered at 385 °C for 2 h.

Table 5 Fracture toughness of ADI-1 and ADI-2

Heat treated condition	K_{Ic}, MPa $\sqrt{m}$
ADT-1	
A	55.2
B	63.1
C	54.9
D	44.1
ADI-2	
G	55.2
H	62.5
I	49.6
J	40.0

ture of 871 °C for 2 h and then austempered at 260 °C for different time periods, such as 5 min, 10 min, 15 min, 30 min, 45 min, 1 h, 2 h, 3 h, 4 h, 5 h, and 6 h. This was done for both ADI-1 and ADI-2. These specimens were then metallographically polished and etched with a 2% nital solution. The volume fractions of ferrite and austenite were then determined in these samples using a PGT Imagist-II (Princeton Gamma Tech, Princeton, New Jersey) image analyzer as well as by x-ray. The volume fractions of ferrite were then plotted (Fig. 5) against the log of austempering time in seconds to examine the nature of growth kinetics of ferrite in these alloys.

3. Results and Discussion

3.1 *Influence of Heat Treatment on Microstructure of ADI*

Figures 3(a) to (d) and 4(a) to (d) show the microstructures of ADI-1 and ADI-2 resulting from various heat treatments. These microstructures are for tensile and fracture toughness samples. Specimens austempered at lower temperature (260 °C) had acicular ferrite, which appears similar to martensitic structure in steel. These are shown in Fig. 3(a) and 4(a). On the other hand, when specimens are austempered at a higher austempering temperature (385 °C), they have coarse ferrite (shown in Fig. 3d and 4d) in microstructures. Results reported in Table 4 show that the amount of austenite in the matrix in-

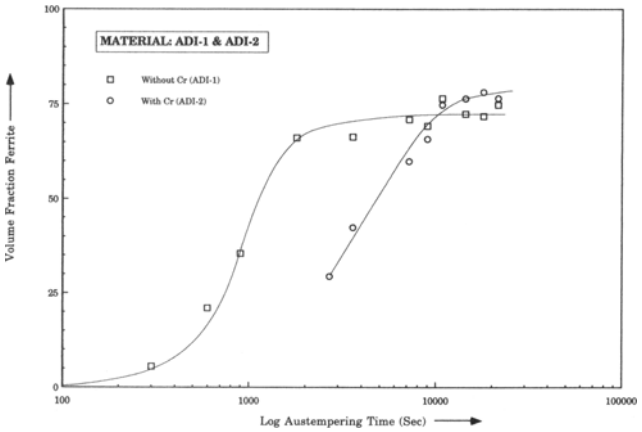

Fig. 5 Austempering time vs. volume fraction of ferrite.

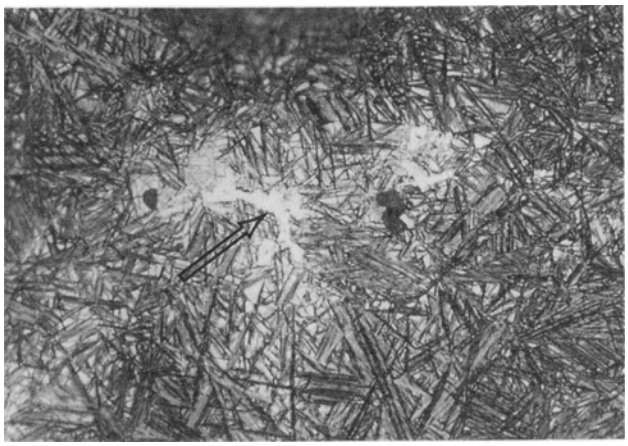

Fig. 6 Microstructure showing segregated region in ADI without Cr. Heat treated condition A. Austempered at 260 °C for 4 h. 1000×.

Fig. 7 Microstructure showing segregated region in ADI with Cr. Heat treated condition G. Austempered at 260 °C for 4 h. 1000×.

creases with the increase in austempering temperature, while the volume fraction of ferrite decreases. In other words, the higher austempering temperatures produce more austenite (Fig. 3d and 4d) and less ferrite, whereas lower austempering temperatures result in more ferrite (Fig. 3a and 4a) and less austenite in the matrix. Test results, reported in Table 4 also show that the addition of Cr did not affect significantly the volume fractions of these phases when austempered at the same temperature. This is interesting because it implies that the presence of chromium did not affect the nucleation and growth of ferrite in these specimens.

The analysis of the microstructure also shows that austenite occurred mainly in the form of slivers (white areas) between adjacent ferritic needles (Fig. 3a and 4a) but changed to a more equiaxed (Fig. 3d and 4d) form with increased austempering temperature. As the austempering temperature has increased, the coarseness of the entire ferritic structure has also increased. Also, some segregation was observed in these specimens. Figures 6 and 7 show the segregated regions as observed under the optical microscope in ADI-1 and ADI-2 when austempered at higher austempering temperature. This light-colored phase was analyzed by electron dispersive analysis by x-ray (EDXA) and was found to consist of various elements, like Si, C, Mo, and Mn, for ADI-1 whereas for ADI-2 it also contained some Cr.

As mentioned earlier, Fig. 5 reports the plot of volume fraction of ferrite vs. the log of austempering time in seconds for ADI-1 and ADI-2 (kinetic samples). The S-shaped nature of the curves in this figure indicates that the transformation reaction during austempering is a nucleation and growth process. Incidentally, this observation is fully supported by the results reported by some earlier workers (Ref 13). Detailed analysis showed ferrite grains are first nucleated at the prior austenitic grain boundaries, which serve as nucleation sites for the heterogeneous nucleation. This will be reported in detail in a later publication. Test results reported in Fig. 5 show another interesting feature. It is evident that the presence of Cr reduced the transformation of austenite to ferrite at lower time periods, whereas at longer time periods, Cr addition helped in growth of more ferrite at this temperature (260 °C).

Since the transformation of austenite into ferrite and carbon-saturated austenite during austempering of ductile cast iron occurs by nucleation and growth (Ref 18) processes, the microstructure of ADI produced by austempering becomes strongly dependent on the transformation temperature. A lower austempering temperature results in large undercooling of the austenite and a slower carbon diffusion rate. Thus, at lower austempering temperature, the nucleation of the ferrite platelets rather than their growth is being favored. Nucleation rate depends on undercooling temperature like supercooling temperature in the case of solidification process. For ferrite grains to grow, carbon must diffuse out fast to provide room for growth. On the other hand, if carbon diffusion is slow (as it is at lower austempering temperature), the ferrite growth is retarded. As a result, austempering at lower temperatures (260 and 288 °C) produced more and finer grained ferrite (Fig. 3a, 3b, 4a, and 4b) with less volume fractions of austenite. At higher austempering temperature, undercooling is lower, and at the same time, the carbon diffusion is fast. Therefore, ferrite grain growth is substantially enhanced. Consequently, the vol-

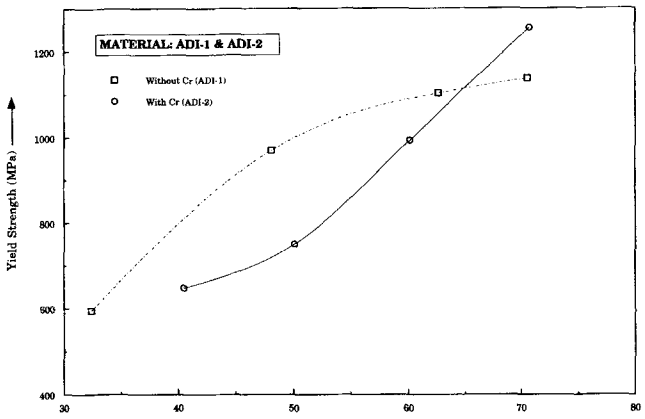

Fig. 8 Influence of volume fraction of ferrite on yield strength of ADI.

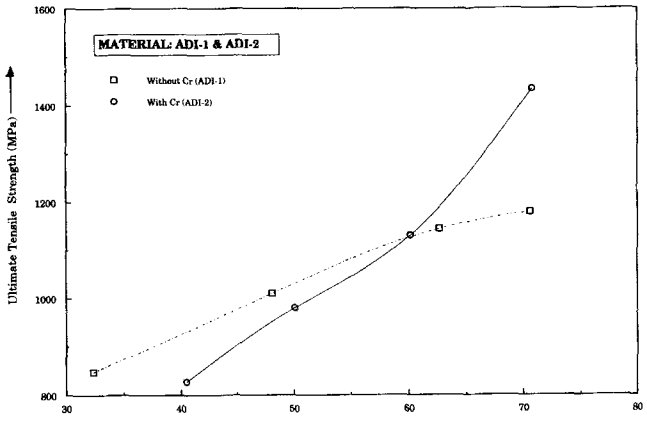

Fig. 9 Influence of volume fraction of ferrite on ultimate tensile strength of ADI.

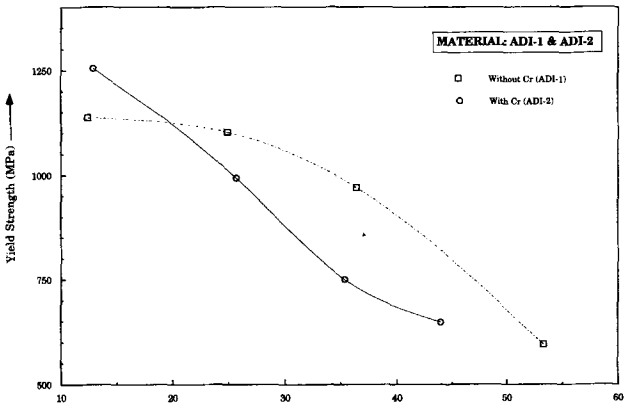

Fig. 10 Influence of volume fraction of austenite on yield strength of ADI.

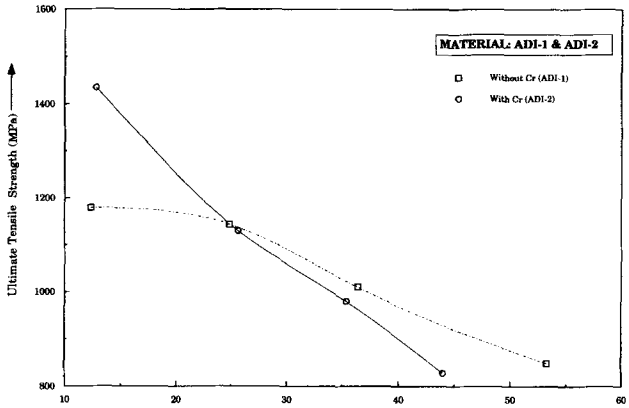

Fig. 11 Influence of volume fraction of austenite on ultimate tensile strength of ADI.

ume fraction of ferrite is smaller, but the individual rod-like ferritic grains are larger in size. These gradual changes can be clearly seen by comparing the microstructures in Fig. 3(a) to (d) and 4(a) to (d). The growth of the nucleated ferrites rather than the nucleation of ferrite is favored at higher austempering temperatures, whereas at lower austempering temperature, nucleation of ferrite is more favorable.

The above results can be summarized as follows: at lower austempering temperature, more ferrite is nucleated, and the growth rate of the ferrite phase is slow. Hence, it results in a larger volume fraction of ferrite in the matrix but with smaller size ferritic grains or platelets. On the other hand, at higher austempering temperature, less ferrite is nucleated, but the growth rate of this ferrite phase is very rapid. Consequently, when ADI is austempered at higher austempering temperature, the matrix contains a lower volume fraction of ferrite, but these ferritic grains or platelets are significantly larger in size.

Another important microstructural change occurs during the austempering process. This is related to the austenite grains. With an increase in the austempering temperature, both the size and shape of the austenite grains are affected. At lower austempering temperatures, the austenite occurs mainly with wedge-like appearance (Fig. 3a and b) between adjacent ferritic plates. This provides a shorter diffusion path for carbon atoms as they are rejected from ferrite (because of the reduced size of this wedge-type austenite). Hence the austenite formed at lower austempering temperature is relatively uniform in carbon content because carbon does not have to move too far, and thus the austenite becomes fully carbon stabilized and uniform in carbon content. This causes these materials to have desirable high strength due to the uniform carbon content of the austenite phase. Hence, for very high strength, ADI should have larger volume fraction of ferrite; at the same time, austenite should be uniformly stabilized with carbon.

At higher austempering temperature, a more blocky shaped austenite is formed between the bundles or colonies (Fig. 3d and 4d) of the rod- or bar-shaped ferrite. Other workers (Ref 19) have also reported similar observations. Due to the large size, these randomly distributed and blocky equiaxed austenite regions will be relatively nonuniform in carbon content because carbon has to diffuse through a larger distance. This nonuniform carbon content of austenite apparently contributes to the lower strength of ADI when austempered at higher austempering temperature.

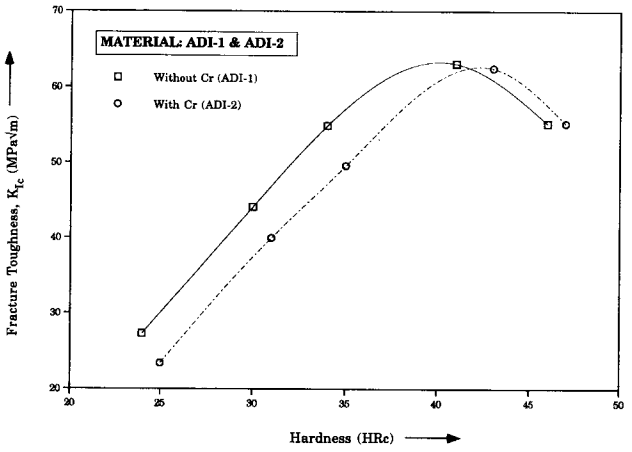

Fig. 12 Influence of hardness on fracture toughness of ADI.

3.2 *Influence of Microstructure on Tensile Properties of ADI*

In Table 3, the tensile properties of ADI-1 (conventional) and ADI-2 (alloyed with Cr) in as-cast as well as after four different heat treatments are reported. These data show that austempering at a lower temperature (260 °C) produced maximum yield and tensile strengths for both ADI-1 and ADI-2. Moreover, austempering at a lower temperature produces minimum ductility. Ductility in ADI increases with the rise in austempering temperature.

In Fig. 8, the yield strengths of ADI-1 and ADI-2 are plotted against volume fractions of ferrite, whereas in Fig. 9 the ultimate tensile strengths are plotted against volume fraction of ferrite. It is evident from these figures that as the volume fractions of ferrite increase, both yield and tensile strengths of ADI-1 and ADI-2 increase. However, increase is much more rapid in the case of ADI with chromium. Therefore, for higher strength, ADI should have higher volume fractions of ferrite; it is achieved by austempering at lower temperatures. However, for higher ductility, ADI should be austempered at a higher temperature, and the ferrite content must be less. In other words, it should have more austenite in the matrix. The higher ductility in the heat treated conditions D and J (Table 3) is an example; i.e., they have larger volume fractions of the austenite phase in the matrix and have more ductility.

The yield and ultimate tensile strengths of ADI-1 and ADI-2 are plotted against volume fractions of austenite in Fig. 10 and 11. These figures clearly show that in both cases as the volume fraction of austenite increases, the yield and tensile strength of both alloys decreases. In other words, for high tensile and yield strength, the ADI should have a lower volume fraction of austenite in the matrix. Comparing the test results in Table 3, it also becomes obvious that the addition of Cr increased the yield and tensile strengths of the material when austempered at the same lower austempering temperature (260 °C) and for the same period of time. However, this effect was not significant because the ratio of the austenite to ferrite volume fraction during the austempering process did not change significantly with the Cr addition. However, segregation was found to be greater in ADI-2. This indicates that the addition of chromium will promote more segregation in ADI.

As mentioned earlier, when an ADI alloy is austempered at a lower austempering temperature (heat treated condition A and G, Table 2), it has a high volume fraction of ferrite with a fine-grained lath microstructure. These fine-grained ferrite and austenite microstructures (Fig. 3a and 4a) produce significant lattice mismatch (Ref 20-23) between the bcc ferrite and fcc austenite phases. Moreover, austenite ADI is more uniform in carbon content when austempered at a lower austempering temperature. This combination is responsible for the very high hardness and very high strength of ADI in heat treated conditions A and G.

3.3 *Influence of Microstructure on Fracture Toughness of ADI*

Table 5 reports the fracture toughness values of ADI-1 and ADI-2. The present test results show that the fracture toughness of ADI is comparable to that of plane carbon and low alloy steels (Ref 15). Since both ADI and plane carbon steels have similar fracture toughness, ADI can be used to replace these materials. ADI will provide an additional advantage in structural design because the manufacturing cost of ADI is lower than that of plane carbon or low alloy steels (Ref 5).

One very interesting observation was made during this study, and it relates to the fracture toughness of other ferrous materials. The fracture toughness of both ADI-1 and ADI-2 increased with the increase in hardness up to about 40 HRC as reported in Table 5. In other materials, the fracture toughness generally decreases as the hardness is increased. Thus, a unique opportunity exists for this engineering material because hardness, strength, and fracture toughness can be increased simultaneously with the heat treatment process in ADI, which is not possible in other materials.

The fracture toughness of ADI-1 and ADI-2 is plotted against the Rockwell C hardness in Fig. 12. It is evident that the maximum fracture toughness in both ADI-1 and ADI-2 is obtained around the hardness level of approximately 40 HRC. Either below or above this hardness level, the fracture toughness of ADI tends to decrease for both ADI-1 and ADI-2. The higher fracture toughness of both ADI-1 and ADI-2 in heat treated conditions B and H (40 HRC) is related to the fact that at this temperature, the austenite formed is fully stabilized (Ref 23) with carbon. On the other hand, at a hardness level below 40 HRC, the microstructure contains some unreacted, i.e., untransformed austenite (Ref 24). This untransformed austenite can transform into stress-induced martensite during the loading process. This causes lower fracture toughness in ADI when austempered at higher austempering temperatures (conditions (C, D, I, and J).

Furthermore, addition of CR has in fact reduced the fracture toughness of ADI at lower hardness levels, whereas at or above 40 HRC, the fracture toughness of both alloys are very similar.

In Fig. 13 and 14, the fracture toughnesses of ADI-1 and ADI-2 are plotted against the volume fraction of ferrite and austenite. Figure 13 shows that as the volume fraction of the ferrite phase increases, the fracture toughness of the material also increases and reaches a peak value when volume fraction of ferrite is around 60%. Above this value, the fracture tough-

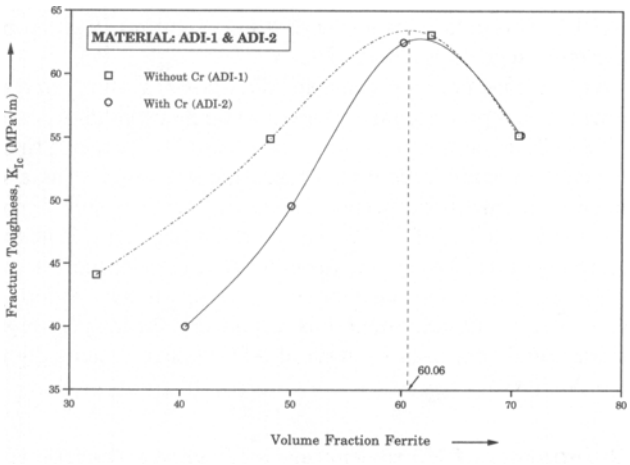

Fig. 13 Influence of volume fraction of ferrite on fracture toughness of ADI.

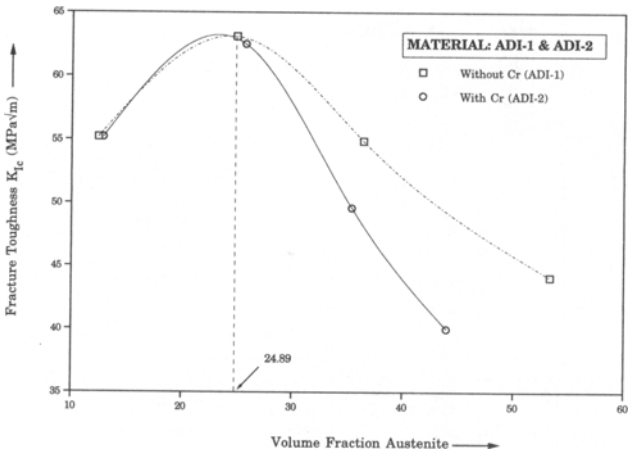

Fig. 14 Influence of volume fraction of austenite on fracture toughness of ADI.

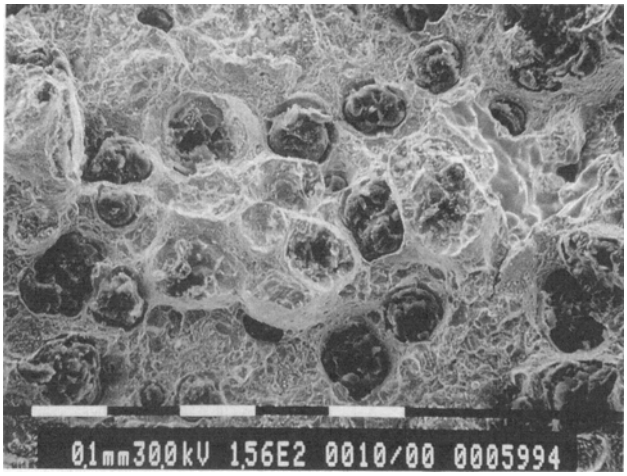

Fig. 15 Typical fractograph of ADI without Cr. 150×. Heat treated condition A. Austempered at 260 °C for 4 h.

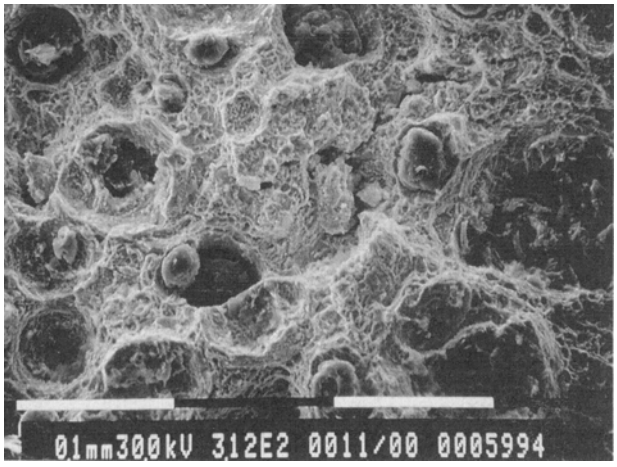

Fig. 16 Typical fractograph of ADI without Cr. 300×. Heat treated condition A. Austempered at 288 °C for 3.5 h.

ness of ADI starts to decrease with the increase in volume fraction of ferrite.

Test results reported in Fig. 14 show that the maximum fracture toughness is attained in both ADI-1 and ADI-2 when the austenite volume fraction is around 25% in the matrix. Thus, the present test results (Table 5) show that for maximum fracture toughness, ADI should have about 60% ferrite and approximately 25% austenite in the matrix.

Typical fractographs of ADI-1 and ADI-2 after different heat treatments are shown in Fig. 15 through 22. Specimens austempered at similar temperatures had similar fracture surface appearances. The purpose of showing these similar fractographs is that even though the metallurgically polished and etched microstructures of the various heat treated conditions are vastly different, the fracture surfaces appear to be the same, i.e., a mixture of quasi-cleavage and ductile microvoids are visible on the fractographs. The fracture plane through the graphite nodules is also clearly shown in these figures, and the shear plane of the nodules is uniformly flat.

The matrix of ADI can withstand a certain amount of deformation before fracturing as it becomes evident from the ductility of the material (Table 3). Since graphite nodules in the matrix cannot deform, they pose as barriers for the matrix deformation and give rise to crack initiations. The graphite nodules are discontinuities in the ADI matrix and produce much higher stresses around themselves. The first step is that the interface around graphite nodules is plastically deformed during loading. This gives rise to the formation of microvoids at the

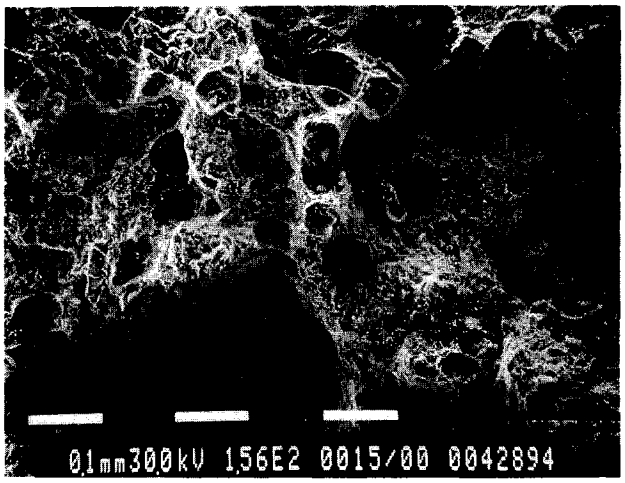

Fig. 17 Typical fractograph of ADI without Cr. 150×. Heat treated condition C. Austempered at 358 °C for 2.5 h.

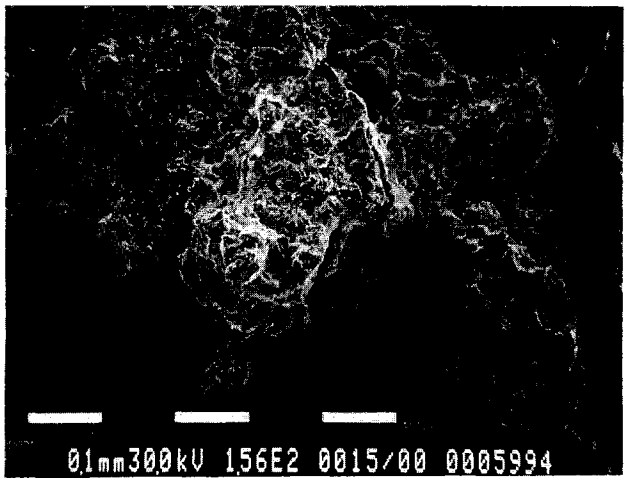

Fig. 18 Typical fractograph of ADI without Cr. 150×. Heat treated condition D. Austempered at 385 °C for 2 h.

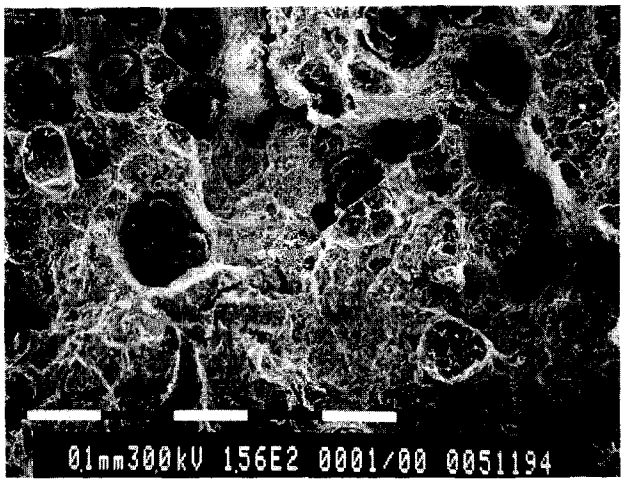

Fig. 19 Typical fractograph of ADI with Cr. 150×. Heat treated condition G. Austempered at 260 °C for 4 h.

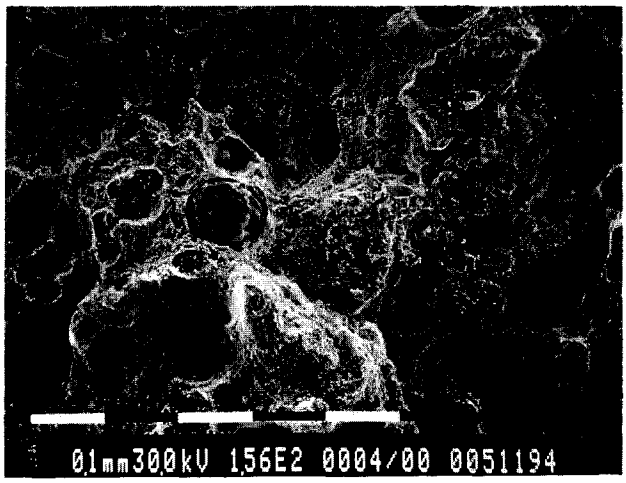

Fig. 20 Typical fractograph of ADI with Cr. 150×. Heat treated condition H. Austempered at 288 °C for 3.5 h.

graphite/ matrix interfaces, which then develop into cracks in the matrix adjacent to the graphite nodules.

Fracture toughness of ADI with Cr was generally lower at higher austempering temperature because chromium produced more segregation in ADI when austempered at higher austempering temperature. These segregations are known to reduce (Ref 26-27) the fracture toughness of ADI alloys. The elements, such as Si and Mn, lead to excessive interdendritic segregation (Ref 28), and they help carbides to form. This carbide precipitates in the intercellular and interdendritic region (Ref 29) and form brittle networks, which is the apparent cause of the reduction in fracture toughness. As mentioned above, in the

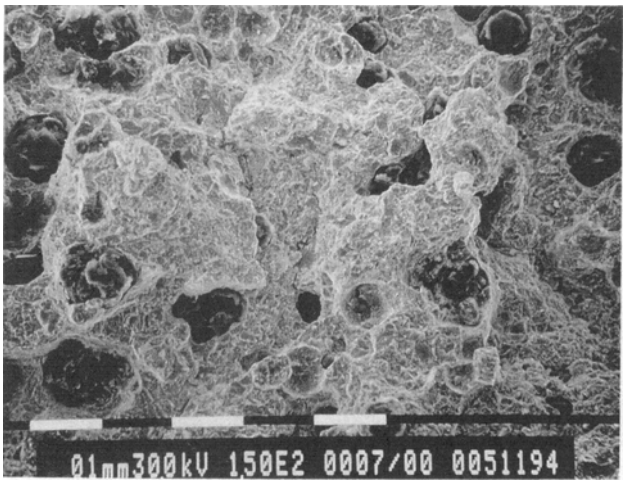

Fig. 21 Typical fractograph of ADI with Cr. 150×. Heat treated condition I. Austempered at 358 °C for 2.5 h.

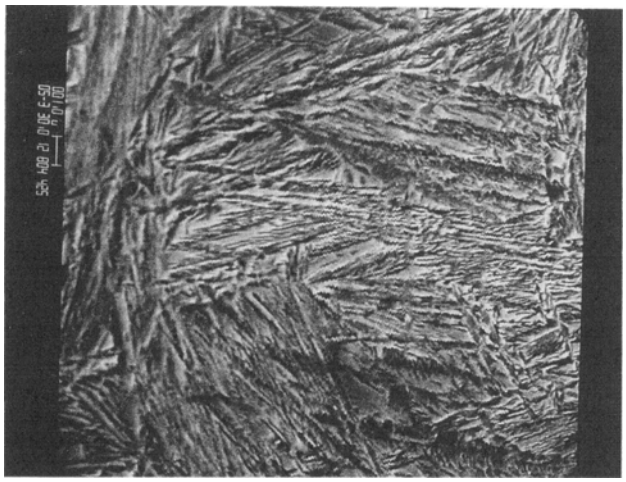

Fig. 23 Scanning electron microscope picture of the segregated region (without Cr). 5000×.

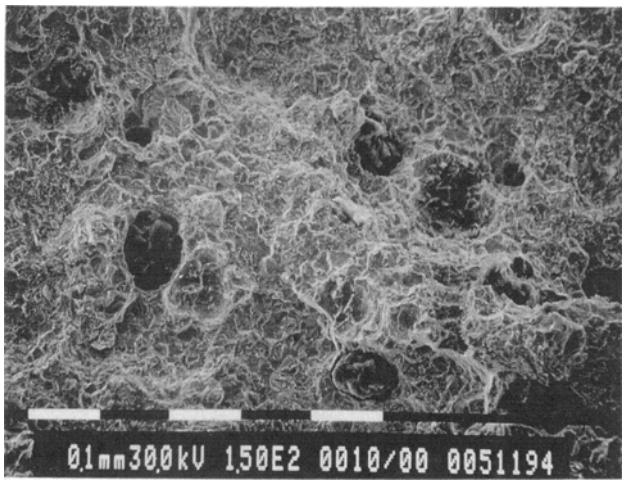

Fig. 22 Typical fractograph of ADI with Cr. 150×. Heat treated condition J. Austempered at 385 °C for 2 h.

presence of Cr, the segregation is more prevalent, and more segregations occur in ADI when austempered at higher austempering temperature. This has caused the reduction of the fracture toughness of ADI-2 at lower hardness levels (heat treated conditions I and J).

The SEM micrograph of the segregated region at a higher magnification is shown in Fig. 23. Microchemical analysis of the area indicates that the elements are mainly Cr, Mn, Mo, and V carbides. These eutectic carbides have an orthorhombic type of crystal structure, which is closely related to cementite. Thus, alloying of ADI with elements Cr, Mn, V, and Mo can cause segregation of these (alloying) elements. The segregation takes place in the intercellular region and may also lead (during the solidification and through precipitation) to unwanted eutectic carbide formation. By reducing the amount of eutectic carbides, the fracture toughness of ADI could possibly be further improved. Perhaps the reduction of eutectic carbides could be attained by slower cooling of the molten metal because the segregation of lower melting point carbides is more likely to be inhibited.

4. Conclusions

- The transformation of austenite to ferrite in ADI occurs by nucleation and growth process.
- Both yield and tensile strength of ADI increases with the increase in volume fraction of ferrite. On the other hand, the ductility of ADI increases with the increase in volume fraction of austenite in the matrix.
- Both yield and tensile strength of ADI decrease with the increase in austempering temperature and with the increasing volume fraction of the austenite in the matrix.
- Fracture toughness of ADI is the highest at or around 40 HRC, or when the alloy contains approximately 60% ferrite and 25% austenite in the matrix. For the optimized fracture toughness, ADI should therefore be austempered at about 280 °C for 3.5 h.
- The addition of Cr to the alloys increased the yield and tensile strength of ADI. However, at the lower (<40 HRC) hardness levels, the fracture toughness of ADI with Cr was

lower than for ADI without Cr. This is apparently due to more segregation in ADI with Cr when austempered at higher austempering temperature.

References

1. J. Dodd, High Strength, High Ductility Ductile Cast Irons, *Mod. Cast.*, Vol 68, 1978, p 60-66
2. E. Dorazil, B. Barta, E. Munsterova, L. Stransky, and A. Huvar, High Strength Bainitic Ductile Cast Iron, *AFS Int. Cast Met. J.*, Vol 7, 1983, p 52-62
3. B.V. Kovacs, Austempered Ductile Cast Iron, Facts and Fiction, *Mod. Cast.*, Vol 36, 1990, p 38-41
4. J.F. Janowak and P.A. Morton, A Guide to Mechanical Properties Possible by Austempering 1.5% Ni 0.3% Mo, *AFS Trans.*, Vol 88, 1985, p 123-135
5. B.V. Kovacs, J.R. Keough, and D.M. Pramstaller, "Austempered Ductile Cast Iron (ADI) Process Development," Gas Research Institute, Jan 1989
6. R.B. Gundalach and J.F. Janowak, Austempered Ductile Cast Iron Combine Strength with Toughness and Ductility, *Met. Prog.*, Vol 12, 1985, p 231-236
7. J.F. Janowak and R.B. Gundalach, Development of a Ductile Iron for Commercial Austempering, *AFS Trans.*, Vol 86, 1983, p 377-388
8. T. Strikawa, On the Austempering Ductile Cast Iron, Their Mechanical Properties and Some Practical Applications, *59th Japan Ductile Cast Iron Association Licensee Conference* (Tokyo), 1978, p 138-150
9. D.J. Moore, T.B. Nouns, and K.B. Rundman, The Relationship Between the Microstructure and Tensile Properties in Austempered Ductile Cast Irons, *AFS Trans.*, Vol 87, 1987, p 165-174
10. T.B. Nouns, K.B. Rundman, and D.J. Moore, On the Structure and Properties of Austempered Ductile Cast Iron, *AFS. Trans.*, Vol 84, 1984, p 115-140
11. J.F. Janowak, R.B. Gundalach, G.T. Eldis, and K. Rohrig, Technical Advances in Cast Iron Metallurgy, *AFS Int. Cast Met. J.*, Vol 6, 1982, p 28-42
12. M. Greech, P. Bowen, and J.M. Young, Effect of Austempering Temperature on the Fracture Toughness and Tensile Properties of an ADI Alloyed with Copper and Nickel, *Second World Conference on ADI* (Ann Arbor, MI), B.V. Kovacs, et al., Ed., 1992, p 135-148
13. D.J. Moore, T.N. Rouns, and K.B. Rundman, The Effect of Heat Treatment, Mechanical Deformation and Alloying Elements on Additions on the Rate of Bainite Formation in Austempered Ductile Irons, *J. Heat Treat.*, Vol 4 (No. 1), 1985, p 7-24
14. E-399, *Annual Book of ASTM Standards*, Vol 03.01, ASTM, 1992, p 745-756
15. R.W. Hertzberg, *Fatigue and Fracture Mechanics of Engineering Materials*, 3rd ed., John Wiley & Sons, 1986
16. G.E. Dieter, *Mechanical Metallurgy*, 3rd ed., McGraw Hill, 1990
17. E 8, *Annual Book of ASTM Standards*, Vol 03.01, ASTM, 1992, p 344-345
18. I. Lemay, *Mechanical Metallurgy*, 2nd ed., Prentice Hall, 1984, p 362
19. M. Johannson, Properties and Applications of Austempered Austenitic Bainitic Ductile Cast Iron, Paper No. 22, *45th International Foundry Congress* (Budapest), 1978
20. L. Bartosiewicz, A.R. Krause, B.V. Kovacs, and S.K. Putatunda, Fatigue Crack Growth Behavior of Austempered Ductile Cast Iron, *AFS Trans.*, Vol. 92, 1992, p 135-142
21. L. Bartosiewicz, A.R. Krause, I. Singh, and S.K. Putatunda, Influence of Microstructure on High Cycle Fatigue Behavior of Austempered Ductile Cast Iron, *Mater. Charact.*, Vol 30, p 221-234, 1993
22. S.K. Putatunda, A. Sengupta, D. Dusaiswany, and L. Bartosiewicz, Near Threshold Fatigue Crack Growth Behavior of Austempered Ductile Cast Iron, *Morris E. Fine Symposium*, P.K. Liaw, Ed., TMS, 1991, p 176-181
23. K.H. Gahr, Fracture Analysis of White Cast Iron, *Z. Metallkd.*, Vol 71 (No. 2), 1980, p 103-112
24. Z.K. Fan and R.E. Smallman, Some Observations on the Fracture of Austempered Ductile Cast Iron, *Scr. Metall. Mater.*, Vol 31 (No. 1), 1994, p 137-142
25. J.M. Schissler and J. Saverna, Segregation Effects on the Formation of Austempered Ductile Cast Iron, *Proceedings of the 1st International Conference on Austempered Ductile Iron* (Chicago), American Society for Metals, 1984, p 70-82
26. M. Gagne, *AFS Trans.*, Vol 93, 1985, p 801-812
27. E. Dorazil, T. Podrabsy, and J. Svejcar, *AFS Trans.*, Vol 98, 1990, p 765-774
28. G.P. Faubert, D.J. Moore, and K.B. Rundman, *AFS Trans.*, Vol 99, 1991, p 831-843
29. M. Nili, Ahmadabadi, T. Ohide, and E. Niyama, *Trans. Jpn. Foundrymen's Soc.*, Vol 11, 1992, p 40-47